Open Access

Jan Osman*, Friederike Großmann, Kay Brosien, Ulrich Kertzscher, Leonid Goubergrits and Thomas Hildebrandt

Assessment of nasal resistance using computational fluid dynamics

DOI 10.1515/cdbme-2016-0136

Abstract: Anterior rhinomanometry is the current gold standard for the objective assessment of nasal breathing by determining the nasal resistance. However, computational fluid dynamics would allow spatially and temporally well- resolved investigation of additional flow parameters. In this study, measured values of nasal resistance are compared with measured values. An unclear discrepancy between the two methods was found, suggesting further investigation.

Keywords: computational fluid dynamics; nasal breathing; nasal resistance; rhinomanometry.

1 Introduction

The human nose plays a substantial role in respiration as well as olfactory and gustatory sensation. Its purpose is not only to condition and cleanse inhaled air, but also to facilitate a transnasal airstream which contributes to maintaining the inner milieu of the nasal cavity and thus the noses' function [1].

Impaired nasal breathing is a frequent issue in otorhinolaryngology with high prevalence in all demographic groups. The reasons that may lead to perception of impaired nasal breathing are manifold and range from disturbed flow or neurologic problems to psychological issues. Thus, identifying a specific cause of the perception of impaired nasal breathing is often difficult. While there are diagnostic tools for spatially well-resolved examination of the nasal cavity's geometry [e.g. X-ray computed tomography (CT), acoustic rhinometry] as well as test kits for olfactory and trigeminal function, there is no spatially resolved method for assessment of nasal airflow, yet. The current gold standard in the assessment of nasal airflow is the anterior rhinomanometry (RMM). This method allows assessment of the nasal resistance of both sides of the nose as function of the volume flow rate through that side of the nose. Subsequently, the total nasal resistance can be calculated from those measured unilateral resistances. This method allows only the calculation of an integral measurement, however.

Therefore, utilization of computational fluid dynamics (CFD) for assessment of nasal airflow might be an essential step toward better understanding of the nose's function as well as treatment of impaired nasal breathing. CFD was already used for investigation of several aspects of nasal breathing: identification of common flow patterns as well as parameters associated with impaired nasal breathing, optimization of drug application via the nose and patient-specific treatment planning [2–7].

Incorporation of CFD into clinical routine might improve diagnosis and treatment within the near future. However, even though substantial progress was made in the understanding of nasal airflow using CFD as well as in-vitro experiments (excellently summarized in [8]), it is of utmost importance to validate CFD against the current gold standard RMM to ensure a good acceptance of this method in a clinical setting.

This project's aim was to validate CFD-derived flow resistances with RMM measurements of the same patients.

2 Material and methods

For a preliminary experiment, three subjects were chosen from existing, retrospective data. For these patients, RMM measurements were available as well as CT image data.

***Corresponding author: Jan Osman,** Charité – Universitätsmedizin Berlin, Biofluid Mechanics Laboratory, Augustenburger Berlin, Germany, E-mail: jan.osman@charite.de
Friederike Großmann, Kay Brosien, Ulrich Kertzscher and Leonid Goubergrits: Charité – Universitätsmedizin Berlin, Biofluid Mechanics Laboratory, Augustenburger Berlin, Germany, E-mail: a.f.r.grossmann@gmx.de (F. Großmann); KayBrosien@posteo.de (K. Brosien); Ulrich.Kertzscher@charite.de (U. Kertzscher); leonid.goubergrits@charite.de (L. Goubergrits)
Thomas Hildebrandt: Limmatklinik, Zurich, Switzerland, E-mail: th@dr-hildebrandt.ch

2.1 Rhinomanometric measurements

RMM was performed using a *4RHINO* system (Rhinolab GmbH, Freiburg, Germany). During the RMM measurements, one nostril was closed using a piece of tape. A tube, piercing the tape, allowed measurement of the static pressure within the closed side of the nose. This pressure is equal to the pressure within the nasopharynx where both sides of the nasal cavity merge. A simplified illustration of this design is shown in Figure 1.

At least five breathing cycles were measured for each side of the nose. Pressure and volume flow rate were recorded every 5 ms. Only measurements of the left nasal cavity were available for the second patient.

Commonly, the volume flow rate (Q) at a pressure drop ($\triangle p$) of 150 pascal is used for calculation of flow resistance ($R = \triangle p/Q$) and thus evaluation of the obstruction of that side of the nose [10]. The total resistance (R_{tot}) induced by the nasal cavity can be described as two individual flow resistances in a parallel setup. Analog to electrical circuits, the total resistance is then defined as:

$$R_{tot} = (R_{left} \cdot R_{right})/(R_{left} + R_{right}). \quad (1)$$

2.2 X-ray computed tomography (CT)

CT image acquisition was performed using a Toshiba Aquilion 64 scanner (Nasu, Japan) at a resolution of 0.25 mm · 0.25 mm · 0.4 mm. This resolution was shown to be sufficient for geometry reconstruction and subsequent CFD use [11].

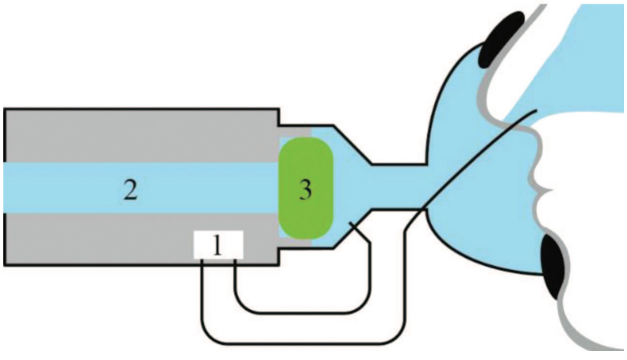

Figure 1: Simplified scheme of the RMM system used. The difference pressure between the ambient within the mask and the closed side of the nose is measured (1). The volume flow rate passing through the open side of the nose is measured within the mouthpiece (2) after passing a filter (3) (based on [9]).

2.3 Segmentation and mesh generation

The geometries of all three nasal cavities were segmented using ZIBAmira (version 2015.28; Zuse Institute Berlin, Germany). While methods such as radio density thresholding and region growing algorithms were used, the segmentation process was performed mostly manually. The nasal cavity was truncated at the nostrils as well as at the pharynx at the height of the larynx. Nasal sinuses as well as ethmoidal air cells were excluded from the segmentation.

Surface geometries were then generated from the final segmentation and smoothed using ReMESH (version 2.0, IMATI, Genoa, Italy). These surfaces were imported into StarCCM+ (version 10.06, CD-adapco, Melville, USA). Using StarCCM+ a polyhedral volume mesh was generated. The node distance of the meshes was 0.4 mm. A boundary layer consisting of three prism layers featuring a total thickness of 36.4% of the node distance was specified. This mesh resolution was shown to be suited for numerical investigation of nasal airflow [12].

2.4 Numerical simulations

Numerical simulations were performed using StarCCM+. Air was modelled as a Newtonian fluid with a constant density of $\rho = 1.225\ \mathrm{kg/m^3}$ and a viscosity of $\eta = 17\ \mu\mathrm{Pa}$.

The walls of the nasal cavity were assumed to be rigid, and a no-slip boundary condition was applied. To ensure comparability to RMM measurements, one nostril was closed, while the other one was specified as a pressure outlet with the target pressure set to zero. At the pharynx a constant velocity boundary condition was set. The velocities were set in such a way, that the resulting inspiratory and expiratory flow rates were equal to those measured at a pressure drop of 150 pascal during RMM. Thus, four steady simulations per patient were performed.

Since the nasal airflow during restful breathing only features transitional turbulence, turbulence was modelled using a standard k-ω-SST model with a low turbulence intensity of 2%.

Simulations were considered converged when residuals reached a limit of 10^{-5} and pressure values, monitored at randomly chosen points, were constant. The pressure drop across the open side of the nose was calculated as the difference of the surface averaged static pressure at the open nostril and the pharynx.

If both methods are able to correctly predict the pressure drop across the nasal cavity – and thus the nasal resistance – they should yield the same results.

3 Results

The unilateral resistances measured during RMM at a pressure drop of 150 Pascal are specified in Table 1. While patient 3 was symptom-free, patients 1 and 2 suffered from impaired nasal breathing. According to RMM, as well as the patient's self-assessment, patient 1 had a severe obstruction of the left side of the nose, resulting in a resistance of more than 5 Pa/ml at a flow rate of only 28 ml/s. The range of measured flow rates at a pressure drop of 150 pascal was 28 ml/s to 490 ml/s.

The corresponding flow rates were then used to specify the inflow boundary conditions of all simulations. The pressure drop across the nasal cavity was then calculated. The resulting unilateral resistances of the simulations are specified in Table 2. The static pressure distribution at the wall of the nasal cavity of patient 2 is shown in Figure 2.

The median resistance of the simulations is $R_{CFD} = 0.047$ Pa/ml with resistances ranging from 0.02 to 0.12 Pa/ml. In all simulations, the calculated pressure drops, and therefore the predicted unilateral resistances, are more than one order of magnitude smaller than the unilateral resistances measured using RMM. Therefore, CFD significantly underestimates the nasal resistance measured using RMM.

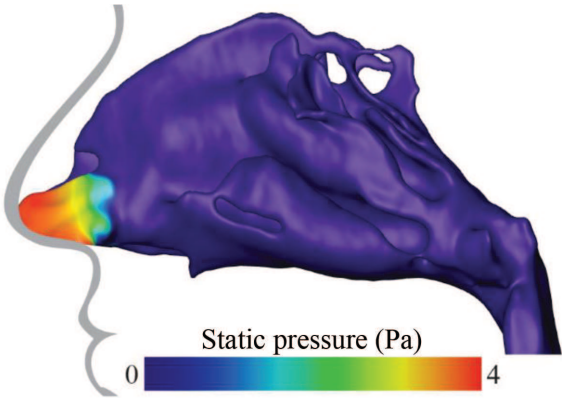

Figure 2: Example of the calculated static pressure distribution for the geometry of the second patient's nasal cavity. A distinct pressure drop can be observed at the nasal isthmus behind the left nostril.

4 Discussion

In a multi-centric study, Vogt et al. evaluated nearly 37,000 RMM measurements using a device similar to the one used in the present study [10]. The RMM results obtained in the present study agree well with the measurements of Vogt et al. Therefore, possible errors associated with numerical studies were analysed.

Limitations, assumptions and boundary conditions of the methods used in this study have previously been thoroughly evaluated by several groups. Truncating the nasal cavity at the nostrils and excluding the ambient was shown to have no severe effect on predicted pressure drop over the nasal cavity [13]. Doorly et al. were able to show good agreements of flow fields calculated using CFD with those measured in-vitro using Particle Image Velocimetry [8]. The quasi-steady assumption, i.e. simulating only a stationary moment of the breathing cycle, was shown to be a valid assumption [8, 14]. According to Fodil et al. ignoring tissue elasticity does not result in gross differences in predicted pressure drop for flow rates observed during restful breathing [15]. Furthermore, we examined the effect of shrinking the nasal cavity, altering the radio density threshold during segmentation and adding a mask to the computational domain. Neither of these alterations caused relevant differences in the pressure drops.

Additionally, the CFD-derived nasal resistance values match those obtained in several other CFD studies of nasal airflow. Hemtiwakorn et al. for example reported calculated flow resistances of approximately 0.03 Pa/ml, while RMM measurements predicted resistances an order of magnitude higher [5]. Even in patients with severe nasal obstruction, nasal resistance values calculated using CFD are usually smaller than 0.2 Pa/ml [16, 17] and are thus much smaller than the values measured using RMM [10]. Nasal resistances calculated using CFD were found to

Table 1: Unilateral resistances in Pa/ml at a pressure drop of 150 pascal measured during inspiration and expiration using rhinomanometry.

Patient	Inspiration		Expiration	
	Left	Right	Left	Right
1	5.35	0.52	5.17	0.55
2	1.29	–	1.07	–
3	0.31	0.36	0.32	0.40

Table 2: Unilateral resistances in Pa/ml calculated at the flow rates measured during RMM at a pressure drop of 150 Pascal.

Patient	Inspiration		Expiration	
	Left	Right	Left	Right
1	0.031 (28)	0.036 (286)	0.040 (29)	0.053 (270)
2	0.017 (116)	–	0.029 (140)	–
3	0.055 (490)	0.120 (415)	0.070 (468)	0.110 (374)

Those flow rates are specified within brackets in ml/s.

usually be smaller than 0.05 Pa/ml in a review by Kim et al. [18].

Thus, the bias between CFD and RMM seems to be a common problem. Therefore, further careful investigations addressing the numerical approach as well as RMM are indicated.

5 Conclusion

Severe differences between nasal resistances measured using RMM and calculated using CFD were found in this study, as well as within existing literature.

While RMM correlates well with impaired nasal breathing, it is limited to an integral measurement of total nasal resistance. However, it is the current gold standard in the assessment of nasal function.

Furthermore, methods used for numerical assessment of nasal airflow are well understood and validated using *in-vitro* experiments. However, it appears that the calculation of nasal resistance using CFD often leads to a gross underestimation of nasal resistance compared to *in-vivo* measurements.

The suspicion that CFD is not suited for calculation of nasal resistances might arise, since RMM is thoroughly embedded in clinical routine. Nonetheless, calculation of pressure drop using CFD is usually a reliable method as well. Therefore, it is unclear, whether RMM measurements alter the breathing behaviour or the airflow in a way that is not yet well understood. Additional research is clearly needed to determine the cause of these differences.

Acknowledgment: The authors would like to thank the Rhinolab GmbH for providing a 4RHINO system at the Park-Klinik Weißensee, Berlin, which will be helpful in further investigations.

Author's Statement

Research funding: The author state no funding involved. Conflict of interest: Authors state no conflict of interest. Material and methods: Informed consent: Informed consent has been obtained from all individuals included in this study. Ethical approval: The research related to human use complies with all the relevant national regulations, institutional policies and was performed in accordance with the tenets of the Helsinki Declaration, and has been approved by the authors' institutional review board or equivalent committee.

References

[1] Hildebrandt T, Heppt WJ, Kertzscher U, Goubergrits L. The concept of rhinorespiratory homeostasis – a new approach to nasal breathing. Facial Plast Surg. 2013;29: 85–92.

[2] Tarabichi M, Fanos N. Finite element analysis of airflow in the nasal valve. Acta Otolaryngol. Head Neck Surg. 1993;19:638–42.

[3] Zhao K, Jiang J. What is normal nasal airflow? A computational study of 22 healthy adults. Int Forum Allergy Rhinol. 2014;4:435–46.

[4] Zhao K, Jiang J, Blacker K, Lyman B, Dalton P, Cowart BJ, et al. Regional peak mucosal cooling predicts the perception of nasal patency. Laryngoscope. 2014;124:589–95.

[5] Hemtiwakorn K, Mahasitthiwat V, Tungjitkusolmun S, Hamamoto K, Pintavirooj C. Patient-specific aided surgery approach of deviated nasal septum using computational fluid dynamics. IEEJ Trans. 2015;10:274–86.

[6] Kimbell JS, Segal R, Asgharian B, Wong BA, Schroeter JD, et al. Characterization of deposition from nasal spray devices using a computational fluid dynamics model of the human nasal passages. J Aerosol Med. 2007;20:59–74.

[7] Tian L, Inthavong K, Lidén G, Shang Y, Tu J. Transport and deposition of welding fume agglomerates in a realistic human nasal airway. Ann Occup Hyg. 2016;1–17.

[8] Doorly DJ, Taylor DJ, Schroter RC. Mechanics of airflow in the human nasal airways. Respir Physiol Neurobiol. 2008;163:100–10.

[9] RhinoLab GmbH, 4Rhino Operation Manual.

[10] Vogt K, Wernecke KD, Behrbohm H, Gubisch W, Argale M. Four-phase rhinomanometry: a multicentric retrospective analysis of 36,563 clinical measurments. Eur Arch Otorhinolaryngol. 2016;273:1185–98.

[11] Quadrio M, Pipolo C, Corti S, Lenzi R, Messina F, Pesci C, et al. Review of computational fluid dynamics in the assessment of nasal air flow and analysis of its limitations. Eur Arch Otorhinolaryngol. 2014;271:2349–54.

[12] Kimbell JS, Garcia GJM, Frank DO, Cannon DE, Pawar SS, Rhee JS. Computed nasal resistance compared with patient-reported symptoms in surgically treated nasal airway passages: a preliminary report. Am J Rhinol Allergy. 2012;26:e94–8.

[13] Taylor DJ, Doorly DJ, Schroter RC. Inflow boundary profile prescription for numerical simulation of nasal airflow. J R Soc Interface. 2010;7:515–27.

[14] Shi H, Kleinstreuer C, Zhang Z. Laminar airflow and nanoparticle or vapor deposition in human nasal cavities with wall roughness. J Aerosol Sci. 2006;38:398–419.

[15] Fodil R, Brugel-Ribere L, Croce C, Sbirlea-Apiou G, Larger C, Papon JF, et al. Inspiratory flow in the nose: a model coupling flow and vasoerectile tissue distensibility. J Appl Physiol. 2005;98:288–95.

[16] Rhee JS, Cannon DE, Frank DO, Kimbell JS. Role of virtual surgery in preoperative planning. Arch Facial Plast Surg. 2012;14:354–9.

[17] Zhu JH, Lee HP, L KM, Lee SJ, San LT, Wang de Y, et al. Inspirational airflow patterns in deviated noses: a numerical study. Comput Methods Biomech Biomed Eng. 2013;16:1298–306.

[18] Kim SK, Na Y, Kim JI, Chung SK. Patient specific CFD models of nasal airflow: overview of methods. J. Biomech. 2013;46:299–306.